A New Algorithm for Determining the Noise Equivalent Delta Temperature of In-Orbit Microwave Radiometers

John Xun Yang, *Senior Member, IEEE*, and Hu Yang, *Member, IEEE*

***Abstract*— The noise equivalent delta temperature (NEDT) determines the radiometric resolution of a radiometer. Determining NEDT is indispensable for assessing the in-orbit radiometer performance and quantifying uncertainty propagation from radiance to climate data records. Agencies of EUMETSAT, UK MetOffice, and National Oceanic and Atmospheric Administration (NOAA) have developed their own algorithms for calculating and monitoring NEDT of in-orbit microwave radiometers. These algorithms are an essential means for monitoring NEDT and hardware health. While remarkable accomplishments have been made, there appears to be room for improvement. The investigation is needed for the NEDT underestimate found at channels like G-band that has pronounced $1/f$ noise. Also, it is necessary to explain the inconsistency in calculated NEDTs of different algorithms. We have reviewed the theoretical basis for determining NEDT and developed an improved algorithm of clear physics and mathematics. We have developed methods for handling error sources that can result in either negative or positive biases with an overall underestimate of NEDT. We have done comparison and validation with the prelaunch thermal vacuum chamber (TVAC) test, in-orbit data, and simulation. The new algorithm significantly improves the estimate of NEDT, including the G-band and advances the understanding of algorithm structures and physical foundations. It can accurately monitor in-orbit NEDT and facilitate quantifying the associated uncertainty propagation through science products.**

***Index Terms*— Microwave radiometry, noise equivalent delta temperature (NEDT), remote sensing, satellite, uncertainty quantification.**

I. Introduction

THE noise equivalent delta temperature (NEDT) represents the radiometric resolution and sensitivity of a radiometer [1], [2]. It is also called equivalent noise temperature, noise equivalent differential temperature, or some other variants. NEDT is a critical metric that needs to meet the mission requirement for all spaceborne radiometers [3]–[5]. Measuring NEDT allows for monitoring hardware noise and health. The NEDT associated uncertainty not only affects the level-1 radiance/brightness temperature but also propagates through higher level science products, such as climate data records (CDRs) [6], [7]. Such uncertainty is presented for both a single satellite and constellation radiometers with intercalibration [8], [9]. NEDT is also an important parameter in simulating and assimilating satellite data for examining radiometric uncertainty propagation. The accurate measurement and estimate of NEDT are a vital component of uncertainty quantification of satellite-based data records, such as CDR.

Algorithms of calculating NEDT have been developed for in-orbit radiometers by different agencies, including the European Organisation for the Exploitation of Meteorological Satellites (EUMETSAT), the UK Meteorological Office (MetOffice), and the National Oceanic and Atmospheric Administration (NOAA) [10]–[13]. These algorithms have been applied in operation for monitoring in-orbit NEDT of different radiometers. They have played a critical role in diagnosing hardware health and monitoring the long-term changes. At NOAA Center for Satellite Applications and Research (STAR), a dedicated site of Integrated Calibration/Validation System (ICVS) has been developed for monitoring the status, such as NEDT of operational radiometers [14]. NEDT of NOAA's microwave sounders can be found at ICVS near real time with a latency of less than 1 h. The site traffic has over 50 000 visitors per year, showing a pervasive influence and growing interest.

While remarkable accomplishments have been made, there is apparent room for improvement. A notable underestimate of NEDT is found at channels, such as G-band, which is prone to $1/f$ noise [15]; nonnegligible differences of calculated NEDTs have been found between different algorithms [16]; and more explanations are necessary for interpreting traditional algorithm structures and the use of some empirical parameters [10]–[13]. In the study, we aim to explain the observed inconsistency and develop an improved algorithm that has clear physics and mathematics. The remainder of this article proceeds as follows. We will first review the theoretical basis for determining NEDT in Section II. In Section III, the new algorithm is introduced. We will lay out the algorithm structure and explain how it can deal with different error sources that can result in either negative or positive biases. The comparison and validation with the thermal vacuum chamber (TVAC), in-orbit data, and simulation are presented in Section IV. We will compare observations with theoretical analyses. Section V concludes the study with a discussion. The traditional algorithms are presented in the Appendix.

Manuscript received April 20, 2021; revised June 22, 2021; accepted July 12, 2021. This work was supported by the National Oceanic and Atmospheric Administration (NOAA) through the Cooperative Institute for Satellite Earth System Studies (CISESS) under Grant NA19NES4320002. *(Corresponding author: John Xun Yang.)*

The authors are with the Earth System Science Interdisciplinary Center (ESSIC)/Cooperative Institute for Satellite Earth System Studies (CISESS), University of Maryland, College Park, MD 20740 USA (e-mail: jxyang@umd.edu).

Digital Object Identifier 10.1109/TGRS.2021.3097594

II. Theory Review

We first review the theoretical basis of NEDT. An algorithm for deriving NEDT should be consistent with the theory with a solid foundation of physics and mathematics.

The power a radiometer antenna receives and delivers to the receiver is [1]

$$P_A = k \cdot T_A \cdot B \tag{1}$$

where P_A is the antenna power, k is Boltzmann's constant, T_A is the antenna temperature, and B is the bandwidth. T_A includes both incoming radiance and the antenna self-emission, which, in practice, is an average of noisy signals accompanied with measurement uncertainty.

The radiometric resolution is the measurement sensitivity of T_A. It can be quantified by estimating the uncertainty of T_A that can be rewritten as

$$T_A = T_{A,\text{ideal}} + \Delta T_A \tag{2}$$

where $T_{A,\text{ideal}}$ is an ideal term that is noise free and ΔT_A is the uncertainty term.

NEDT represents ΔT_A and can be determined by the second moment of ΔT_A by [1]

$$\text{NEDT}^2 = \int {\Delta T_A}^2(t)dt. \tag{3}$$

The equation is written as a function of time. An equivalent but a different form in the frequency domain is sometimes used per Parseval's theorem [2] that we will introduce shortly.

The antenna temperature can be related to the measured count as

$$(T_A + T_R)G = C \tag{4}$$

where T_R is the receiver temperature, C is the measured count, and G is the power gain. The system temperature is the summation of the antenna and receiver temperature

$$T_{\text{sys}} = T_A + T_R. \tag{5}$$

To appreciate variables affecting NEDT, the uncertainty of the system temperature ΔT_{sys} is written as [1]

$$\Delta T_{\text{sys}} = T_{\text{sys}}\left(\frac{1}{B\tau} + \frac{\Delta G}{G}\right)^{\frac{1}{2}} \tag{6}$$

where $T_{\text{sys}} = T_A + T_R$, and T_R is the receiver temperature. G is the power gain with its fluctuation as ΔG. We see that the radiometric resolution is affected by the bandwidth B, the integration time τ, and the gain fluctuation ΔG.

Hersman and Poe [2] proposed a variant form of ΔT_{sys} written in the frequency domain instead of the time domain

$$\Delta T_{\text{sys}}^2 = c^2 \int_0^\infty df S_r(f)H(f) \tag{7}$$

where c is a constant, $S_r(f)$ is the radiometer characteristics power spectrum in the frequency domain, and $H(f)$ is the transfer function describing the periodic calibration. One of the purposes of the modified form is to emphasize the impact of periodic calibration. Furthermore, the thermal noise exhibits a different power spectrum from $1/f$ noise in the frequency domain as shown in the study of Hersman and Poe [2]. Examining noise in the frequency domain can discriminate noise from a unique perspective different from the time domain. We will utilize the power spectrum for characterizing noise and comparing algorithms.

III. NEDT Algorithm for in-Orbit Radiometers

A. Algorithm Overview

We have developed an algorithm for determining the NEDT of in-orbit radiometers. The algorithm takes the strength of traditional algorithms and has a physical substance with a bunch of error sources removed. We take the Advanced Technology Microwave Sounder (ATMS) onboard Suomi National Polar-orbiting Partnership (SNPP) as an example since it has carried out thorough TVAC tests [10], [17], [18]. It has also gone through careful calibration and inter calibration [19], [20]. Its in-orbit status, including NEDT, is continuously monitored as can be found in NOAA's ICVS site (www.star.nesdis.noaa.gov/icvs/) [14].

The earth scene temperature has a large dynamic range. Extracting noise, ΔT_A, from the earth scenes is difficult and yields large errors. The warm-load antenna temperature can be used instead since it is more stable and can be measured by PRT [10]–[13]. In the meantime, it is necessary to remove a bunch of error sources for an accurate estimate, such as the warm-load orbital oscillation.

The warm-load count is related to its incoming radiance as

$$\left(T_{A,W} + T_R\right)G = C_W \tag{8}$$

where $T_{A,W}$ is the warm-load antenna temperature, C_W is the warm-load count, and G is the power gain.

Likewise, the cold-space count is

$$(T_C + T_R)G = C_C \tag{9}$$

where T_C is the cosmic background temperature and C_C is the cold-space count. We write the cosmic temperature as T_C rather than $T_{A,C}$ since the cosmic temperature is used as a reference for calibration, which is often a constant in practice.

To reduce noise, the gain is derived with smoothed counts of several scanning periods. Fig. 1 shows the diagram of scans in the cross-track and along-track directions and the smoothing window. The smoothed cold-space count is

$$\overline{C_{Ck}} = \frac{1}{M(2n+1)} \sum_{j=k-n}^{k+n} w_j \sum_{i=1}^{M} C_{Ci,j} \tag{10}$$

where i is for the cross-track scan, j is for the along-track scan, and k is the new dummy variable of the along-track scan since the smoothed counts are only dependent on the along-track. M is the number of cross-track scans of warm-load (e.g., $M = 4$ for ATMS). w_j is the window function for the moving average with $2n + 1$ as the window size. It can be either a rectangular or triangular window

$$w_j = \begin{cases} \dfrac{1}{2n+1}, & \text{rectangle} \\ \dfrac{1}{n+1}\left(1 - \dfrac{|j|}{n+1}\right), -n \le j \le n, & \text{triangle.} \end{cases} \tag{11}$$

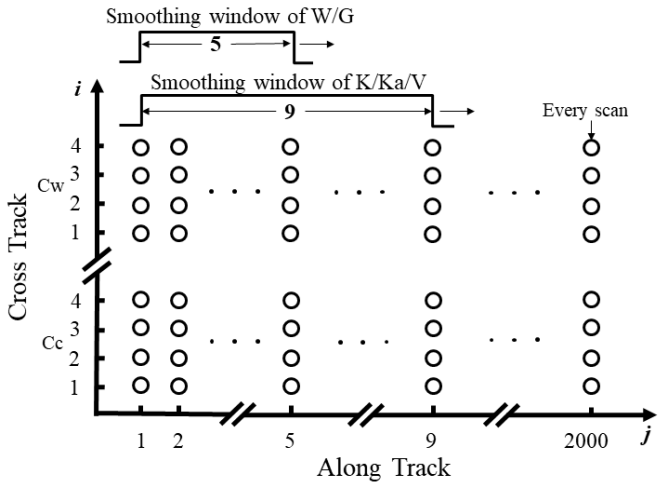

Fig. 1. Diagram of cold-space and warm-load counts in the cross-track and along-track directions. There are ~ 2 000 along-track scans per orbit and four cross-track scans for either the cold or warm counts. A smoothing window is used for deriving the gain with a window length of five and nine along-track scans for the cold and warm counts, respectively.

There is only a negligible difference of a few hundredth Kelvins of NEDT between using the two windows. The window size can be optimized on the ground test. For ATMS, it is determined in the ground TVAC test, which is 9 for channels 1–15 and 5 for channels 16–22, respectively [17]. With respect to the above equation, $n = 4$ for channels 1–15 and $n = 2$ for channels 16–22.

The smoothed warm-load PRT temperature is

$$\overline{T_{Wk}} = \frac{1}{N_{\mathrm{PRT}}(2n+1)} \sum_{j=k-n}^{k+n} w_j \sum_{i=1}^{N_{\mathrm{PRT}}} T_{Wi,j} \tag{12}$$

where N_{PRT} is the number of PRTs used for measuring the warm-load temperature. For ATMS, eight PRTs are used for K-/Ka-/V-bands with five PRTs for W-/G-bands.

The smoothing for the warm-load counts is different from that of cold-space counts. The warm-load counts are divided into two subsets. Doing so can calculate the gain and T_A separately and avoid generating a pseudo-f^2 noise as we will discuss later. For ATMS, the two subsets can be for cross-track scans 1 and 2, and 3 and 4, respectively. Each subset has the same number of along-track scans that have ~ 2 000 scans of one complete orbit. Thus, each subset is a matrix of $2 \times 2\,000$. Specifically, we first smooth C_W that is used for calculating the gain as follows:

$$\overline{C_{Wk}} = \frac{1}{2(2n+1)} \sum_{j=k-n}^{k+n} w_j \sum_{i=3}^{4} C_{Wi,j} \tag{13}$$

where there is $3 \le i \le 4$, indicating a subset of all the four cross-track scans.

The gain is calculated by

$$\overline{G_j} = \frac{\overline{C_{Wj}} - \overline{C_{Cj}}}{\overline{T_{Wj}} - T_C} \tag{14}$$

where the subscript i for cross-track is omitted with j retained, indicating these variables are only dependent on the along-track scan after smoothing. It is noted that the gain is calculated with warm-load counts of the first subset with $3 \le i \le 4$. T_C is a constant, such as 2.73 K for the cosmic background.

The warm-load antenna temperature $T_{A,W}$ is given by

$$T_{A,W_{i,j}} = \frac{1}{\overline{G_j}}\left(C_{Wi,j} - \overline{C_{Cj}}\right) + T_C, \quad 1 \le i \le 2. \tag{15}$$

It is noted that $T_{A,W_{i,j}}$ only has two scans with $1 \le i \le 2$ in the cross-track direction since the other two have been used for calculating the gain.

The derived warm-load antenna temperature contains signals of the orbital oscillation of warm-load temperature that is not noise and should be removed. Since orbital oscillation is well measured by the warm-load PRT, it can be removed by

$$N_{Wi,j} = T_{A,W_{i,j}} - \overline{T_{Wj}} \tag{16}$$

where $N_{Wi,j}$ is the warm-load noise.

NEDT is the square root of the unbiased second central moment

$$\mathrm{NEDT} = \left[\frac{1}{2N-1} \sum_{j=1}^{N} \sum_{i=1}^{2} \left(N_{Wi,j} - \overline{N_W}\right)^2\right]^{1/2} \tag{17}$$

where N is the number of along-track scanline after smoothing with tails removed, and $\overline{N_W} = (1/\mathrm{MN}) \sum_{j=1}^{N} \sum_{i=1}^{M} N_{Wi,j}$. Since there is a total of $2N$ samples, the unbiased estimate has a denominator of $2N - 1$.

In the following, we will discuss the specifics of our algorithm. We will explain why these procedures are crucial for an accurate estimate of NEDT. The pitfalls that can introduce biases will be discussed. We will also compare our algorithm with traditional ones.

B. Removing Orbital Oscillation

In our algorithm, the warm-load orbital oscillation is removed with the PRT temperature as in (16). The removal looks subtle but is important. The environment and status of a radiometer usually have an oscillation as the spacecraft orbits the earth. Fig. 2 shows the warm-load temperature of Suomi NPP ATMS. A notable temperature variation due to the orbit oscillation is observed with the peak-to-peak amplitudes of 0.21 and 0.37 K for the K-/Ka-/V-band and W-/G-band, respectively. The oscillation has a period of ~ 100 minutes as the same as the period of the sun-synchronous orbit of NPP. Such orbital oscillation has been found in all the other radiometers [3], [4], [21], [22].

The orbital oscillation is not noise and has to be appropriately removed from computing NEDT. Since NEDT is often derived from the warm-load temperature with a full orbit, not removing the orbital oscillation would overestimate NEDT. However, the oscillation is not removed in traditional algorithms [11]–[13]. On the other hand, inappropriately removing the orbital oscillation can also result in errors. While the orbital oscillation is a low-frequency signal, the $1/f$ noise can also play a role in the low-frequency regime [15]. A simple cutoff of the low-frequency part of the noise, which intends to reduce the orbital oscillation, will leave noise like $1/f$ uncounted and

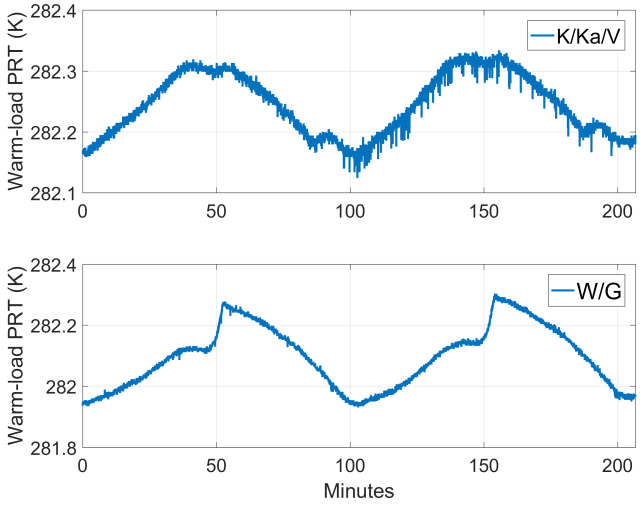

Fig. 2. Orbital oscillation of ATMS warm-load temperature at the K-/Ka-/V-band and the W-/G-band. ATMS has two separate warm-loads: K-/Ka-/V-bands share one warm-load, and W-/G-bands use the other one. The orbital oscillation has the same period of ∼100 min as the spacecraft orbit. It should be removed from computing NEDT since it is not noise.

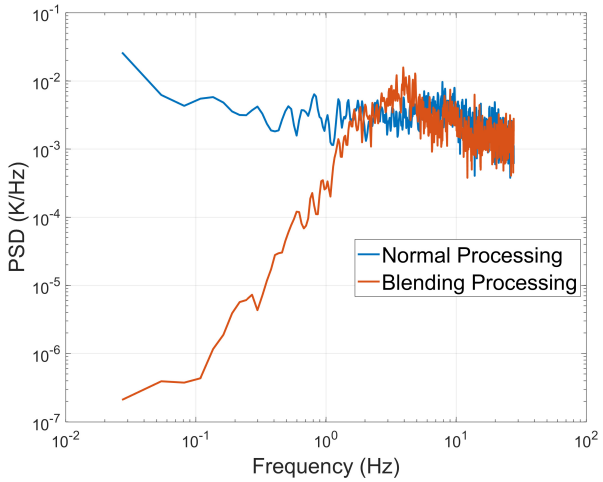

Fig. 3. Power spectrum density of noise of the warm-load antenna temperature at the G-band channel 16 of NPP ATMS. The blue one is from the normal processing by separating warm-load counts for calculating the gain and antenna temperature. The red line is from the blending method where the gain and antenna temperature are not independent of each other. The normal processing shows the thermal noise and $1/f$ noise at the high- and low-frequency regimes, respectively. In contrast, the blending method generates a pseudo-f^2 noise, resulting in an underestimate of NEDT.

underestimate NEDT. We will explain how to deal with the low-frequency noise in the following.

C. Preventing Pseudo-f^2 Noise

Our algorithm separates the warm-load counts to two subsets [see (13)–(15)]. The gain and warm-load antenna temperature are calculated from the two subsets, respectively. The procedures are different from traditional algorithms that blend the calculation of gain and warm-load antenna temperature [11]–[13]. In traditional algorithms, the warm-load counts are smoothed by

$$\overline{C'_{Wk}} = \frac{1}{2(2n+1)} \sum_{j=k-n}^{k+n} w_j \sum_{i=1}^{4} C_{Wi,j} \tag{18}$$

where there is $1 \le i \le 4$ for ATMS, which is different from (13) that only uses cross-track positions of $3 \le i \le 4$. The calculation of G and $T_{A,W}$ also uses $1 \le i \le 4$, and $T'_{A,W}$ in traditional algorithms is given by [11]–[13]

$$T'_{A,W_{i,j}} = \frac{1}{\overline{G_j}}\left(C_{Wi,j} - \overline{C_{Cj}}\right) + T_C, \quad 1 \le i \le 4. \tag{19}$$

The above equation is a blending method that does not discriminate counts for calculating G and $T_{A,W}$. It is different from (14) and (15) that subset warm-load counts and differentiate the derivation of G and $T_{A,W}$. It also differs from the normal operation for deriving the earth-view brightness temperature. In normal processing, the gain is calculated from cold and warm counts without using any of the earth scene counts. The gain and the earth counts that are independent of each other are then used for computing the earth scene temperature.

A pseudo-f^2 noise in the power spectrum can be made up with the blending method. Fig. 3 compares the power spectrum of the two methods. Our method clearly shows the presence of $1/f$ noise at the low-frequency regime, whereas the blending method generates a pseudo-f^2 spectrum. It should be clear that the blending method does not reduce $1/f$ noise. The earth scene brightness temperature still has $1/f$ noise. The pseudo-f^2 noise is simply a false signal due to inappropriate signal processing. The false processing results in an underestimate of the low-frequency noise, such as $1/f$ noise.

The pseudo-f^2 noise can be explained by the Fourier transform. When the gain and scene temperature are derived in a blending way, the scene temperature is mathematically based on the first derivative of counts. Thus, its Fourier transform follows:

$$\mathcal{F}\left(f'(x)\right) = (j\omega)F(\omega) \tag{20}$$

where $f(x)$ is the function for counts, $f'(x)$ denotes the first derivative, ω is the angular frequency, and j is the imaginary number. $F(\omega)$ is the Fourier transform of the function $f(x)$, which is $F(\omega) = \mathcal{F}(f(x))$. The power spectrum $S(\omega)$ is proportional to the square of the Fourier transform

$$S(w) = (j\omega)^2 F^2(\omega). \tag{21}$$

We see that $S(\omega)$ has a multiplicative term of $(j\omega)^2$, which results in the pseudo-f^2 at the low-frequency regime.

D. Using an Unbiased Estimator

An unbiased estimator is employed in our algorithm [see (17)]. This is different from using a biased estimator that can bias the estimate of NEDT. When processing the radiance data, we deal with a discrete and finite sample, which has the *sample variance* [23]. We want the sample variance to be a good estimator of the *population variance* that is for an entire population and can be infinite and continuous. For estimating the variance of noise, there exist two different ways of biased

and unbiased estimators

$$\sigma^2 = \begin{cases} \dfrac{1}{M}\displaystyle\sum_{i=1}^{M}(x_i - \overline{x})^2, & \text{biased} \\ \dfrac{1}{M-1}\displaystyle\sum_{i=1}^{M}(x_i - \overline{x})^2, & \text{unbiased} \end{cases} \tag{22}$$

where σ^2 is the sample variance and $\overline{x_i}$ is the mean such that $\overline{x_i} = (1/M)\sum_{i=1}^{M} x_i$. When M is large enough, there is only a negligible difference between the unbiased and biased estimator. However, a small M can result in a noticeable difference.

We can write the warm-load T_A as

$$T_A = \begin{bmatrix} x_{1,1} & \cdots & x_{1,N} \\ \vdots & \ddots & \vdots \\ x_{M,1} & \cdots & x_{M,N} \end{bmatrix} \tag{23}$$

where the row denotes the cross-track scans and the column is for the along-track.

The following steps have been employed previously [11], [12]:

$$\text{NEDT}_{\text{biased}} = \sqrt{\frac{1}{MN}\sum_{j=1}^{N}\sum_{i=1}^{M}\left(x_{i,j} - \overline{x_j}\right)^2} \tag{24}$$

where $\overline{x_j}$ is the cross-track mean, $\overline{x_j} = (1/M)\sum_{i=1}^{M} x_{i,j}$. This is a biased estimate that underestimates NEDT. An unbiased estimator is

$$\text{NEDT}_{\text{unbiased}} = \sqrt{\frac{1}{(M-1)N}\sum_{j=1}^{N}\sum_{i=1}^{M}\left(x_{i,j} - \overline{x_j}\right)^2}. \tag{25}$$

The difference is in the denominator with $M-1$ substituting M, and the new equation is an unbiased estimate [23]. While there is $M = 4$ for ATMS, using a denominator of $1/M$ instead of $1/(M-1)$ will underestimate NEDT.

Fig. 4 shows the difference between biased and unbiased estimates for NEDT. The thermal noise is generated with the additive white Gaussian noise (AWGN) and added into the warm-load T_A, and the biased and unbiased estimates are illustrated. The bias is a function of cross-track scans M. The negative bias is pronounced with a small M. It can be reduced with a larger M, but the underestimate is persistent.

E. Avoiding a Limited Time and Frequency Scale

In our algorithm, we count the antenna temperature noise in the entire time and frequency domains of the given sample as in (17). On the other hand, biases can be introduced if the noise is estimated with limited time or frequency scales. The radiometer noise has a dependence on frequency and time. At a time scale of a millisecond or less, thermal noise usually dominates. With a larger time scale, $1/f$ noise and orbital oscillations can play a role [2], [15]. This means that NEDT derived from different time or frequency scales can be different. Scale issues occur when NEDT is derived from using a limited time or frequency scale.

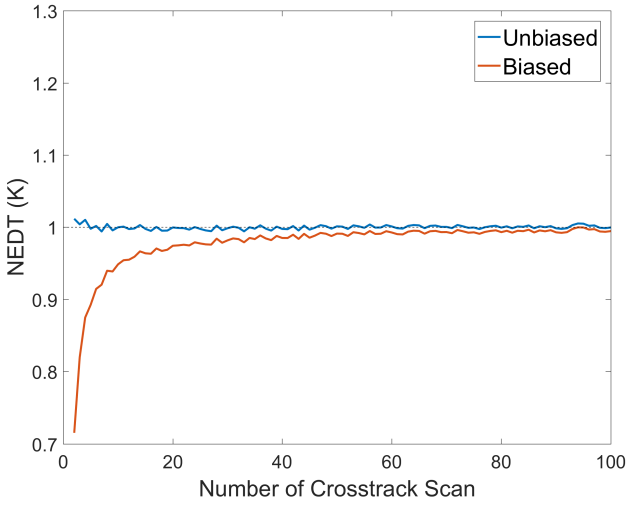

Fig. 4. Biased versus unbiased estimators. The dashed line is the truth. The biased estimator has negative biases that become pronounced with a small number of cross-track scans.

Assuming that the warm-load T_A is a matrix of $[M, N]$ as in (23), NEDT was calculated by steps as follows [11], [12]:

$$\sigma_k^2 = \frac{1}{M(2n+1)}\sum_{j=k-n}^{k+n}\sum_{i=1}^{M}\left(x_{i,j} - \overline{x_k}\right)^2 \tag{26}$$

where $\overline{x_k}$ is

$$\overline{x_k} = \frac{1}{M(2n+1)}\sum_{j=k-n}^{k+n}\sum_{i=1}^{M} x_{i,j}. \tag{27}$$

n is set as 3 in traditional algorithms [11], [12]. This corresponds to 18.7 s for ATMS since the window size has seven along-track scans.

NEDT of a limited time window was derived as [11], [12]

$$\text{NEDT}_{\text{limited}} = \sqrt{\frac{1}{N-2n}\sum_{k=n}^{N-n}\sigma_k^2}. \tag{28}$$

The term σ_k^2 only counts variance in a short window of $2n+1$ along-track scans, that is, 18.7 s. In other words, it only counts the high-frequency noise ($<$18.7 s) while neglecting any low-frequency noise ($>$18.7 s). This can bias NEDT when noise is dependent on the time and frequency scales.

Fig. 5 shows NEDT derived with the afore-said method with three different noises, including thermal, $1/f$, and quantization. The thermal noise is generated with an AWGN generator, and $1/f$ and quantization noises are based on AWGN and Fourier transform [31]. NEDT is calculated with varying cross-track window sizes. The NEDT of thermal noise is insensitive to the window size. This makes sense since thermal noise has a flat power spectrum, and it is independent of frequency and time. In contrast, $1/f$ noise is underestimated with a small time scale that is the high-frequency regime. As the window size increases, the NEDT estimate approaches the truth. Quantization noise is the opposite of $1/f$ noise such that a small time scale overestimates NEDT. This is because quantization noise has an inverse power spectrum.

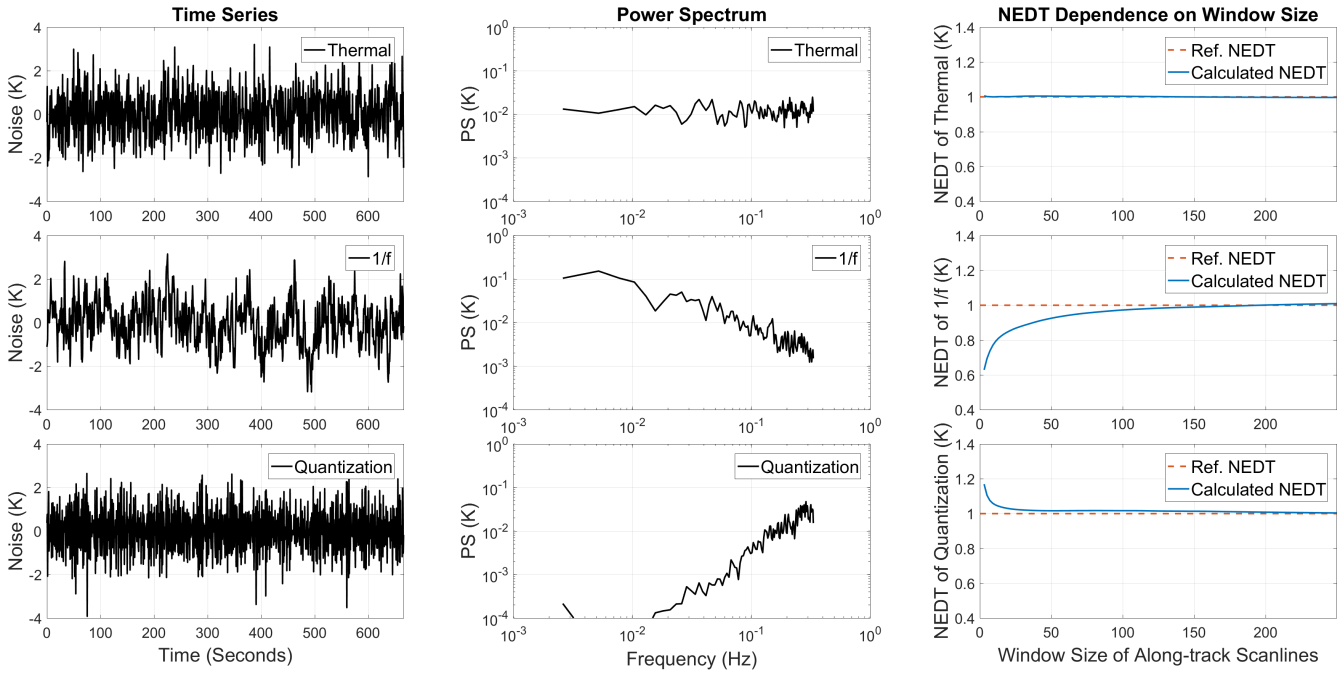

Fig. 5. Different time scales result in different NEDT. For the thermal noise, the NEDT calculation is insensitive to the time scale in terms of the window size. The $1/f$ noise is underestimated with a small time scale that only counts the high-frequency regimes, and conversely, the quantization noise is overestimated with a small time scale.

To summarize, using a limited time and frequency scale can bias NEDT, which can be an overestimate or underestimate depending on noise types. Since $1/f$ noise is more commonly presented in radiometers, a limited small time scale usually results in a negative bias.

F. Comparison Against Algorithms Based on Allan Variance

The Allan variance has been used to calculate NEDT [13], [25]. The Allan variance is a powerful tool in many areas, such as studying frequency instability [26]–[28]. Although our algorithm is not based on the Allan variance, we have investigated specific traditional algorithms for comparison.

The overlapping Allan variance is mostly used since it has an improved statistical confidence over the nonoverlapping one. It can be written by

$$\sigma_x^2(m) = \frac{1}{2m^2(M-2m+1)} \sum_{j=1}^{M-2m+1} \left[\sum_{i=j}^{j+m-1} (x_{i+m} - x_i) \right]^2 \tag{29}$$

where x_i is the sample and M is the number of samples. m is the stride, which is the number of sub-samples in one stride. σ is the Allan deviation equivalent to the square root of the Allan variance. The Allan variance can be denoted as a function of time τ with $\tau = m\tau_0$ and τ_0 of the sampling interval. The overlapping Allan variance provides useful spectral information in the time domain.

When $\tau = \tau_0$ ($m = 1$), the above equation reduces to the two-sample Allan variance as [26]

$$\sigma_x^2 = \frac{1}{2(M-1)} \sum_{i=1}^{M-1} (x_{i+1} - x_i)^2. \tag{30}$$

The two-sample Allan variance is a scalar without spectral information.

The Allan variance is related to the power spectrum as [29]

$$\sigma_x^2(\tau) = 2 \int_0^\infty S(f) |H(f)|^2 \frac{\sin^4(\pi f \tau)}{(\pi f \tau)^2} df \tag{31}$$

where f is the frequency, $H(f)$ is the transfer function of the sensor, and $S(f)$ is the one-sided power spectrum of the time series x.

Different noises can have distinct power spectrum, $S(f)$

$$S(f) = S_0 f^\alpha \tag{32}$$

where S_0 is a constant and α is the power-law exponent. α can be dependent on noise types. For instance, there are $\alpha = -1$ for the $1/f$ noise, $\alpha = 0$ for the thermal noise, and $\alpha = 2$ for the quantization noise.

The Allan spectra of thermal, $1/f$, and quantization noises are [29], [31]

$$\sigma_x(\tau) = \begin{cases} \sqrt{\frac{S_0}{2}} \tau^{-\frac{1}{2}}, & \text{thermal} \\ (2S_0 \ln 2)^{\frac{1}{2}}, & 1/f \\ c_q S_0 \tau^{-1}, & \text{quantization} \end{cases} \tag{33}$$

where c_q is a constant. It is seen that σ_x has a power-law dependence of $\tau^{-(1/2)}$ for thermal noise. This indicates using a large τ will underestimate thermal noise with a power-law decrease. For $1/f$ noise, it is a constant independent of τ. The quantization noise has a power-law exponent of -1 in the Allan spectra.

The two-sample Allan variance does not necessarily represent the sample variance. Rather, it is dependent on the noise

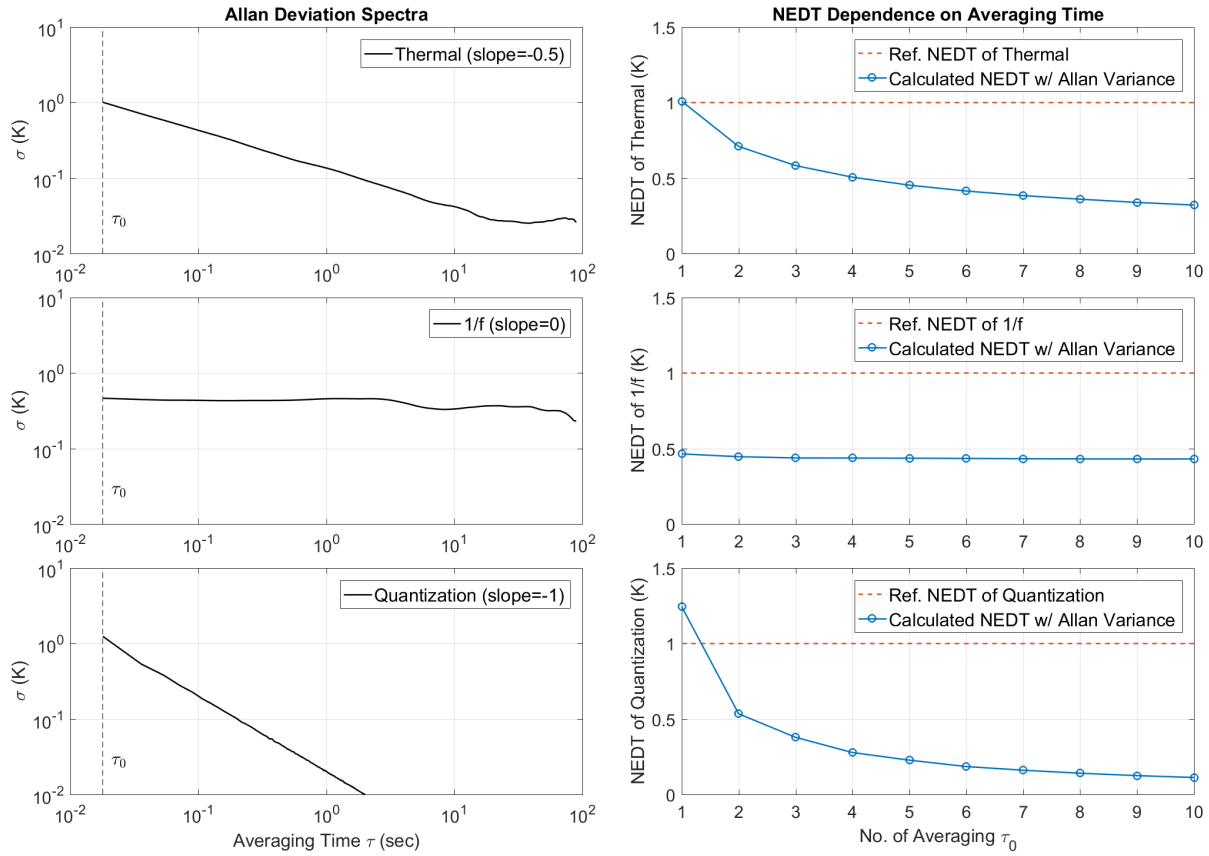

Fig. 6. Allan variance for estimating thermal, $1/f$, and quantization noises. The Allan deviation spectra have a power-law dependence of $\tau^{-1/2}$, τ^0, and τ^{-1} for thermal, $1/f$, and quantization noises, respectively. For the thermal noise, it is only unbiased at $\tau = \tau_0$ and becomes an underestimate as τ increases. For the $1/f$ noise, it always underestimates NEDT. For quantization noise, it is an overestimate with $\tau = \tau_0$ but an underestimate with $\tau > \tau_0$. While the Allan variance was applied to adjacent along-track scans for calculating NEDT [13], [25], it corresponds to $\tau = 4\tau_0$ for ATMS and is an underestimate for thermal, $1/f$, and quantization noises.

types of different noise power spectra. A general relationship between the two-sample Allan variance and the sample variance is

$$\begin{cases} \sigma_x^2(\tau = \tau_0) = \sigma_{ref}^2, & \alpha = 0 \\ \sigma_x^2(\tau = \tau_0) < \sigma_{ref}^2, & \alpha < 0 \\ \sigma_x^2(\tau = \tau_0) > \sigma_{ref}^2, & \alpha > 0 \end{cases} \tag{34}$$

where σ_{ref}^2 is the true sample variance. The two-sample Allan variance can underestimate ($\alpha < 0$) or overestimate ($\alpha > 0$) noise depending on the exponent α of the noise power spectrum. When $\alpha = 0$, the two-sample Allan variance is only unbiased with $\tau = \tau_0$. As τ increases, the Allan variance is an underestimate of the thermal noise following a power law of $\tau^{-1/2}$. Since the $1/f$ noise is very common, the two-sample Allan variance usually underestimates NEDT.

Fig. 6 shows the Allan variance for estimating NEDT with simulated thermal, $1/f$, and quantization noises. We see the Allan spectra have a power-law dependence of $\tau^{-1/2}$, τ^0, and τ^{-1} for the three types of noise, respectively. For the thermal noise, the Allan variance is only unbiased at $\tau = \tau_0$ and becomes an underestimate with τ increasing. For $1/f$ noise, the Allan variance always underestimates NEDT regardless of what τ is used. The quantization noise is overestimated with $\tau = \tau_0$ but underestimated with $\tau > \tau_0$. When NEDT was calculated for adjacent along-track scans [13], [25], it corresponded to a time interval of 2.67 s for ATMS that is $\tau = 4\tau_0$ with τ_0 as the cross-track scan time interval of warm-load scans. This method underestimated NEDT for all of the three noises.

IV. Comparison and Validation

A. Algorithm Structure Comparison

We have examined the theoretical basis and algorithm structures. To accurately estimate the NEDT of in-orbit radiometers, we need to address several error sources, including the orbital oscillation, pseudo-f^2 noise, biases estimator, scale issue, and the use of Allan Variance. The orbital oscillation is not noise and can result in an overestimate of NEDT. The pseudo-f^2 noise underestimates the low-frequency noise, such as $1/f$ noise. A biased estimate results in underestimates of NEDT. Using a small window only counts noise at a small time scale (high-frequency) and neglects the low-frequency noise, such as the $1/f$ noise. The Allan variance is only unbiased for thermal noise with an appropriate time interval. A time interval larger than the sampling interval would underestimate the thermal noise. For the $1/f$ noise, an underestimate is persistent regardless of the time interval used.

TABLE I

ALGORITHM COMPARISON. Y (YES) IS FOR ISSUES WITH THE SIGN FOR POSITIVE (+) OR NEGATIVE (−) BIASES. N MEANS NO ISSUES. WE PREDICT THAT TRADITIONAL ALGORITHMS WILL OVERALL UNDERESTIMATE NEDT AS NEGATIVE BIASES DOMINATE POSITIVE BIASES

Error Sources	EUMETSAT	UK MetOffice	NOAA	New
Orbital Oscillation	Y(+)	Y(+)	Y(+)	N
Pseudo f^2	Y(-)	Y(-)	Y(-)	N
Biased Estimator	Y(-)	Y(-)	Y(-)	N
Scale issue	Y(-)	Y(-)	Y(-)	N
Biased Allan Variance	N	N	Y(-)	N

Table I is a summary of algorithm comparison. Error sources are listed with the sign of biases denoted. The error sources can result in either negative or positive biases that are dependent on noise types and algorithms as we have afore-discussed. The bias signs are predicted from examining the algorithm structures and the theoretical basis of NEDT. Overall, we predict that an underestimate of NEDT is present in traditional algorithms due to the dominating negative biases.

B. Validation Against Simulation

We have done simulations and tested different algorithms. In the simulation, we produce radiometer counts that are used as input for different algorithms. Empirical parameters from observation are used, including the warm-load temperature and the gain. The mean warm-load temperature is 280 K with the mean gain of 15 Count/K and the cosmic background of 2.75 K. Sinusoidal orbital oscillations are added to the warm-load and gain with the magnitudes estimated from observations. We generate $1/f$ and Gaussian noise with known magnitudes and add them into the counts. The percentages of $1/f$ and Gaussian noise are set as 30% and 70%, respectively. The simulation is for one orbit with 2000 along-track scans and four cross-track scans for cold-space and warm-load, respectively.

Different algorithms are applied to estimate NEDT, and the results are shown in Fig. 7. An underestimate of NEDT is found in traditional algorithms. Our new algorithm produces the least error. The simulation results are consistent with the theoretical analysis that predicts an NEDT underestimate of traditional algorithms.

C. Validation Against TVAC

We have compared the derived in-orbit NEDT against TVAC measurements. Suomi NPP ATMS has undergone extensive TVAC measurements with detailed results documented on NOAA STAR site [10], [17], [18]. In TVAC, ATMS is under a controlled environment. The scene targets are cold plates of a set of temperatures of low (80 K), middle (190 K), and high (300 K). ATMS has six redundant configuration (RC) electronic units with RCs 1, 2, 5, and 6 tested [10], [18]. RC1 is used in the in-orbit operation. NEDT is measured in TVAC with the observed uniform scenes. We have compared TVAC-measured NEDT with in-orbit NEDT of different algorithms. The TVAC NEDT of RC1 with the cold plate of 300 K is used since it is the closest to the warm-load temperature.

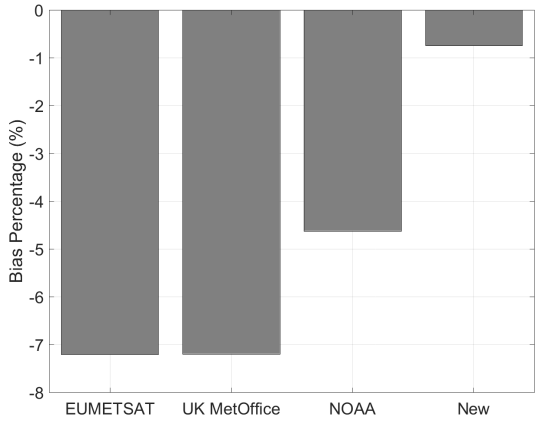

Fig. 7. Comparing different algorithms with simulation. The simulated counts are used as input for different algorithms. Empirical parameters from observation are used, including the warm-load temperature and gain. Sinusoidal orbital oscillations are added to the warm-load temperature and the gain. A blend noise is added in simulation with the $1/f$ and thermal noise of 30% and 70%, respectively. The new algorithm shows superior performance. The results are consistent with the theoretical prediction.

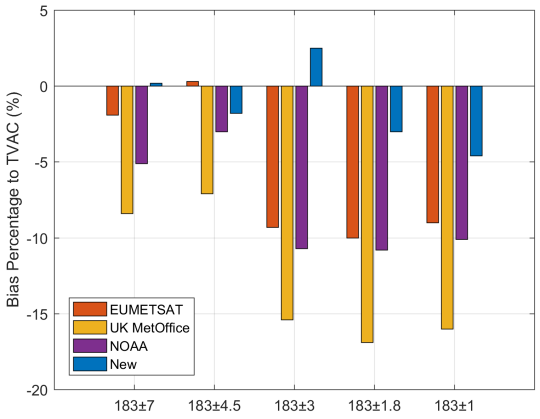

Fig. 8. Comparing NEDTs against TVAC at 183 GHz. The relative error is shown. While the 183 GHz is prone to $1/f$ noise, the new algorithm produces an accurate estimate of NEDT and exhibits consistent performance regardless of the channels and $1/f$ noise.

The TVAC results of NEDT can be found in open-accessible documents of ATMS science meetings on the NOAA STAR website (www.noaa.gov/star) [18].

The NEDT produced by different algorithms is compared to the prelaunch TVAC measurements. A typical comparison is for 183 GHz since it operates at a relatively high frequency that is prone to the occurrence of $1/f$ noise [15]. Different algorithms can have pronounced differences in presence of $1/f$ noise due to their ability to handle it, as found in the theoretical analysis of algorithm structures. Fig. 8 shows the relative error in percentage. Noticeable errors as high as -17% have been found in traditional algorithms. The new algorithm effectively reduces errors. Furthermore, the new algorithm is consistent through all channels regardless of $1/f$ noise.

Table II shows the comparison of all the 22 channels between TVAC and in-orbit measurements. The relative difference of in-orbit NEDT of different algorithms to that of TVAC is shown with a large difference (absolute $>$ 7%) marked in bold. It is seen that large errors are presented at some

TABLE II

COMPARING NEDT OF DIFFERENT ALGORITHMS AGAINST TVAC. LISTED ARE TVAC NEDT (K) AND RELATIVE ERROR (%) WITH LARGE ERRORS (ABSOLUTE VALUE > 7%) MARKED IN BOLD. THE ERRORS OF TRADITIONAL ALGORITHMS ARE PRONOUNCED AT THE G- AND V-BAND CHANNELS 5–7

Channel	TVAC (K)	EUMETSAT (%)	UK MetOffice (%)	NOAA (%)	New (%)
1	0.249	4.8	1.1	-2.1	1.5
2	0.311	**-7.8**	**-12.0**	**-9.1**	0.2
3	0.365	1.5	-3.9	0.4	3.2
4	0.279	1.1	-6.8	0.8	6.5
5	0.278	-5.9	**-13.0**	-5.5	1.3
6	0.289	-1.9	**-9.5**	-5.7	4.7
7	0.271	-4.5	**-10.4**	**-7.4**	-0.1
8	0.267	-1.4	-6.6	-2.1	-1.4
9	0.291	**7.3**	1.1	4.6	4.6
10	0.418	1.5	-4.8	-3.8	3.1
11	0.555	1.5	-3.0	-6.1	-0.3
12	0.574	-0.4	-4.4	-2.7	2.5
13	0.845	**7.4**	3.9	6.7	5.5
14	1.182	-0.5	-3.5	-1.0	5.7
15	1.927	-0.2	-3.2	-1.0	2.1
16	0.285	0.1	-5.2	0.1	1.1
17	0.432	-1.9	**-9.3**	-0.8	-3.8
18	0.371	-1.9	**-8.4**	-5.1	0.2
19	0.432	0.3	**-7.1**	-3.0	-1.8
20	0.501	**-9.3**	**-15.4**	**-10.7**	2.5
21	0.560	**-10.0**	**-16.9**	**-10.8**	-3.0
22	0.712	**-9.0**	**-16.0**	**-10.1**	-4.6
Mean Absolute Error	NA	3.6	**7.5**	4.5	2.7
Max Error	NA	**-10.0**	**-16.9**	**-11.3**	6.5

channels from traditional algorithms. The errors are mostly an underestimate of NEDT. The underestimate has been predicted by the theoretical analysis of algorithm structures. The G-band is most notable with biases as large as -16.9%. Since the G-band operates for high frequencies, the presence of $1/f$ noise can be pronounced [15]. The V-band channels 4–9 also show some noticeable biases from traditional algorithms. The presence of $1/f$ noise at the V-band has also been found in previous studies [30]. The new algorithm shows superior performance through all channels.

V. CONCLUSION

NEDT is a vital metric representing radiometric resolution. Determining NEDT is important for assessing the in-orbit radiometer performance. NEDT is also a key parameter in simulating and assimilating satellite data for quantifying the uncertainty propagation from radiance to CDRs. We have developed a new algorithm for estimating the NEDT of in-orbit microwave radiometers. The algorithm has clear physics and mathematics based on a thorough review of the theoretical basis. It removes error sources that can bias the estimate of NEDT. We have compared the new algorithm against traditional ones with an in-depth analysis of algorithm structure and theoretical basis and illustrate its physical substance.

We have done comparison and validation with TVAC and in-orbit measurements and simulation. The new algorithm exhibits superior performance at all channels, including the G-band, which is prone to $1/f$ noise. While inconsistency and underestimate are found at the G-band in traditional algorithms, our algorithm shows an accurate estimate against TVAC. The results of the new algorithm are consistent between theoretical analysis, observations, and simulation. The new algorithm will be employed for monitoring in-orbit microwave radiometers. The accurate NEDT determination provides critical information for radiometric uncertainty quantification through radiance and climate data.

APPENDIX
ALGORITHMS OF EUMETSAT, UK METOFFICE, AND NOAA

A. EUMESAT

The EUMESAT algorithm for calculating NEDT of in-orbit microwave radiometers is given as follows [12]. The warm-load count is smoothed by

$$\overline{C_{Wk}} = \frac{1}{M(2n+1)} \sum_{j=k-n}^{k+n} w_j \sum_{i=1}^{M} C_{Wi,j} \tag{35}$$

where n denotes the window size of moving average and is set as 3 (window size is $2n+1=7$). M is the number of cross-track warm-load scans. For ATMS, there is $M=4$. The same moving average is applied to the cold-space count and the warm-load PRT temperature. w_j is a triangular window function as

$$w_j = \frac{1}{n+1}\left(1 - \frac{|j|}{n+1}\right), \quad -n \le j \le n. \tag{36}$$

In practice, $n=3$ is used, which is a window size of seven along-track scanlines.

The gain is calculated by

$$\overline{G_j} = \frac{\overline{C_{Wj}} - \overline{C_{Cj}}}{\overline{T_{Wj}} - 4} \tag{37}$$

where the number 4 in the denominator denotes a 4 K cold-space temperature.

The NEDT is

$$\text{NEDT} = \sqrt{\frac{1}{M(N-2n)}\sum_{j=n+1}^{N-n}\sum_{i=1}^{M}\left(\frac{C_{Wi,j}-\overline{C_{Wj}}}{\overline{G_j}}\right)^2} \quad (38)$$

where N is the along-track number of a full orbit.

B. UK Met Office

The UK Met Office has an algorithm in operational use [11], [12]. The same smoothing with a triangular window function of seven along-track scans is applied to the cold, warm counts, and warm-load PRT temperature.

A scalar gain from the average of a full orbital data is used

$$\overline{G} = \frac{1}{M(N-2n)\left(\overline{T_W}-3\right)}\cdot\sum_{j=n+1}^{N-n}\sum_{i=1}^{M}\left(\overline{C_{Wi,j}}-\overline{C_{Ci,j}}\right) \quad (39)$$

where M is cross-track scans ($M = 4$ for ATMS) and N is the number along-track scanlines; 3 is the cold-space temperature. $\overline{T_W}$ is the mean of the warm-load temperature

$$\overline{T_W} = \frac{1}{M(N-2n)}\sum_{j=n+1}^{N-n}\sum_{i=1}^{M}T_{Wi,j}. \quad (40)$$

The cross-track mean is subtracted from the warm-load count

$$\Delta C_{Wi,j} = C_{Wi,j} - \overline{C_{Wj}} \quad (41)$$

where $\overline{C_{Wj}}$ is the cross-track mean.

A scalar warm-load count is defined as

$$\overline{\Delta C_W} = \frac{1}{M(N-2n)}\sum_{j=n+1}^{N-n}\sum_{i=1}^{M}\Delta C_{Wi,j}. \quad (42)$$

Finally, the NEDT is

$$\text{NEDT} = \frac{16}{15}\sqrt{\frac{1}{M(N-2n)}\sum_{j=n+1}^{N-n}\sum_{i=1}^{M}\left(\frac{\Delta C_{Wi,j}-\overline{\Delta C_W}}{\overline{G}}\right)^2}. \quad (43)$$

C. NOAA

An algorithm was developed as the operational algorithm in NOAA STAR [13]. The algorithm is based on the two-sample Allan variance. The gain is calculated by

$$G_{i,j} = \frac{C_{Wi,j}-C_{Ci,j}}{T_{Wi,j}-T_C}. \quad (44)$$

The gain is averaged of the four cross-track scans

$$\overline{G_j} = \frac{1}{4}\sum_{i=1}^{4}G_{i,j}. \quad (45)$$

NEDT is based on the Allan variance

$$\text{NEDT} = \sqrt{\frac{1}{2(N-1)4}\sum_{j=1}^{N-1}\sum_{i=1}^{4}\left(\frac{C_{Wi,j+1}-C_{Wi,j}}{\overline{G_j}}\right)^2} \quad (46)$$

where N is the number of along-track scanlines. The two-sample Allan variance is applied to the warm-load counts of adjacent along-track scans: $C_{Wi,j+1}$ and $C_{Wi,j}$. It corresponds to a sample interval of 2.67 s. Since there are four cross-track warm-load scans in 2.67 s, this corresponds to $\tau = 4\tau_0$ with τ_0 for the time interval of cross-track scans.

REFERENCES

[1] F. T. Ulaby and D. G. Long, *Microwave Radar and Radiometric Remote Sensing*. Ann Arbor, MI, USA: Univ. Michigan Press, 2014.

[2] M. S. Hersman and G. A. Poe, "Sensitivity of the total power radiometer with periodic absolute calibration," *IEEE Trans. Microw. Theory Techn.*, vol. MTT-29, no. 1, pp. 32–40, Jan. 1981.

[3] F. J. Wentz, P. D. Ashcroft, and C. L. Gentemann, "Post-launch calibration of the TRMM microwave imager," *IEEE Trans. Geosci. Remote Sens.*, vol. 39, no. 2, pp. 415–422, Feb. 2001, doi: 10.1109/36.905249.

[4] K. Gopalan, W. L. Jones, S. Biswas, S. Bilanow, T. Wilheit, and T. Kasparis, "A time-varying radiometric bias correction for the TRMM microwave imager," *IEEE Trans. Geosci. Remote Sens.*, vol. 47, no. 11, pp. 3722–3730, Nov. 2009, doi: 10.1109/TGRS.2009.2028882.

[5] E. Kim, C.-H. J. Lyu, K. Anderson, R. V. Leslie, and W. J. Blackwell, "S-NPP ATMS instrument prelaunch and on-orbit performance evaluation," *J. Geophys. Res. Atmos.*, vol. 119, no. 9, pp. 5653–5670, May 2014, doi: 10.1002/2013JD020483.

[6] C. Merchant, G. Holl, J. Mittaz, and E. Woolliams, "Radiance uncertainty characterisation to facilitate climate data record creation," *Remote Sens.*, vol. 11, no. 5, p. 474, Feb. 2019.

[7] T. Popp *et al.*, "Consistency of satellite climate data records for Earth system monitoring," *Bull. Amer. Meteorological Soc.*, vol. 101, no. 11, pp. E1948–E1971, Nov. 2020.

[8] J. X. Yang, D. S. McKague, and C. S. Ruf, "Uncertainties in radiometer intercalibration associated with variability in geophysical parameters," *J. Geophys. Res., Atmos.*, vol. 121, no. 19, pp. 11,348–11,367, Oct. 2016.

[9] W. Berg *et al.*, "Intercalibration of the GPM microwave radiometer constellation," *J. Atmos. Ocean. Technol.*, vol. 33, no. 12, pp. 2639–2654, 2016.

[10] F. Weng *et al.*, "Calibration of Suomi national polar-orbiting partnership advanced technology microwave sounder," *J. Geophys. Res. Atmos.*, vol. 118, no. 19, pp. 11187–11200, 2013, doi: 10.1002/jgrd.50840.

[11] A. Doherty, N. Atkinson, W. Bell, B. Candy, S. Keogh, and C. Cooper, "An initial assessment of data from the advanced technology microwave sounder," Exeter, U.K., Met Office Forecast R&T Rep. 569, Oct. 2012, pp. 2477–2480, vol. 12, no. 12.

[12] N. Atkinson, *NET Specification and Monitoring for Microwave Sounders*, Met Office, Exeter, U.K., 2015.

[13] M. Tian, X. Zou, and F. Weng, "Use of Allan deviation for characterizing satellite microwave sounder noise equivalent differential temperature (NEDT)," *IEEE Geosci. Remote Sens. Lett.*, vol. 12, no. 12, pp. 2477–2480, Dec. 2015, doi: 10.1109/LGRS.2015.2485945.

[14] (2015). *Integrated Calibration/Validation System (ICVS) Overview, ICVS Team*. [Online]. Available: https://www.star.nesdis.noaa.gov/star/

[15] T. H. Lee, *The Design of CMOS Radio-Frequency Integrated Circuits*, 2n ed. Cambridge, U.K.: Cambridge Univ. Press, 2004.

[16] J. Ackermann, "Calculation of noise equivalent temperature variations," EUMETSAT, Telecon Commun., Darmstadt, Germany, Tech. Rep. 1, 2017.

[17] D. Gu, "ATMS striping assessment and mitigation," NGAS SNPP Mission Support Team, Falls Church, VA, USA, Tech. Rep., Dec. 2013.

[18] *STAR Independent Assessment of J1 ATMS Thermal Vacuum Test CP-Mid and CP-High Data Analysis*. STAR ATMS SDR Team. Accessed: May 13, 2014. [Online]. Available: https://www.star.nesdis.noaa.gov/star/

[19] F. Weng, H. Yang, and X. Zou, "On convertibility from antenna to sensor brightness temperature for ATMS," *IEEE Geosci. Remote Sens. Lett.*, vol. 10, no. 4, pp. 771–775, Jul. 2013, doi: 10.1109/LGRS.2012.2223193.

[20] J. X. Yang and H. Yang, "Radiometry calibration with high-resolution profiles of GPM: Application to ATMS 183-GHz water vapor channels and comparison against reanalysis profiles," *IEEE Trans. Geosci. Remote Sens.*, vol. 57, no. 2, pp. 829–838, Feb. 2019.

[21] P. W. Gaiser *et al.*, "The WindSat spaceborne polarimetric microwave radiometer: Sensor description and early orbit performance," *IEEE Trans. Geosci. Remote Sens.*, vol. 42, no. 11, pp. 2347–2361, Nov. 2004, doi: 10.1109/TGRS.2004.836867.

[22] J. R. Piepmeier *et al.*, "SMAP L-band microwave radiometer: Instrument design and first year on orbit," *IEEE Trans. Geosci. Remote Sens.*, vol. 55, no. 4, pp. 1954–1966, Apr. 2017, doi: 10.1109/TGRS.2016.2631978.
[23] G. James, D. Witten, T. Hastie, and R. Tibshirani, *An Introduction to Statistical Learning*. New York, NY, USA: Springer, 2013.
[24] E. A. Lee and P. Varaiya, *Structure and Interpretation of Signals and Systems*, 2nd ed. Reading, MA, USA: Addison-Wesley, 2011.
[25] I. Hans, M. Burgdorf, V. O. John, J. Mittaz, and S. A. Buehler, "Noise performance of microwave humidity sounders over their lifetime," *Atmos. Meas. Techn.*, vol. 10, no. 12, pp. 4927–4945, Dec. 2017.
[26] D. W. Allan, "Time and frequency (time-domain) characterization, estimation, and prediction of precision clocks and oscillators," *IEEE Trans. Ultrason., Ferroelectr., Freq. Control*, vol. TUFFC-34, no. 6, pp. 647–654, Nov. 1987.
[27] D. B. Sullivan, D. W. Allan, D. A. Howe, and F. L. Walls, Eds., "Characterization of clocks and oscillators," NIST, Gaithersburg, MD, USA, Tech. Note 1337, 1990.
[28] N. El-Sheimy, H. Hou, and X. Niu, "Analysis and modeling of inertial sensors using Allan variance," *IEEE Trans. Instrum. Meas.*, vol. 57, no. 1, pp. 140–149, Jan. 2008, doi: 10.1109/TIM.2007.908635.
[29] T. J. Witt, "Using the Allan variance and power spectral density to characterize DC nanovoltmeters," *IEEE Trans. Instrum. Meas.*, vol. 50, no. 2, pp. 445–448, Apr. 2001, doi: 10.1109/19.918162.
[30] N. Bormann, A. Fouilloux, and W. Bell, "Evaluation and assimilation of ATMS data in the ECMWF system," *J. Geophys. Res., Atmos.*, 118, no. 23, pp. 12970–12980, 2013, doi: 10.1002/2013JD020325.
[31] W. J. Riley, "Handbook of frequency stability analysis," NIST, Gaithersburg, MD, USA, Special Publication 1065, 2008.

John Xun Yang (Senior Member, IEEE) received the Ph.D. degree from the University of Michigan, Ann Arbor, MI, USA, in 2015.

He is an Assistant Research Scientist with the Earth System Science Interdisciplinary Center (ESSIC) and the Cooperative Institute for Satellite Earth System Studies (CISESS), University of Maryland, College Park, MD, USA. His research interests include earth remote sensing, microwave radiometry. He has been involved with four NASA/NOAA satellite missions.

Dr. Yang is also a member of the NASA/JAXA Global Precipitation Measurement (GPM) Mission and works on satellite radiometer calibration and science applications. He has done engineering work on building up an L-band radiometer and accessory data acquisition system to calibrate GPS simulators for the NASA Cyclone Global Navigation Satellite System (CYGNSS) Mission. He did multiple field campaigns for the NASA Aquarius mission. He is also a member of the NOAA/NASA Joint Polar Satellite System (JPSS) Mission with a focus on the Advanced Technology Microwave Sounder (ATMS). He was a recipient of the First Place Prize at the 2013 Michigan Geophysical Union (MGU) Symposium, the ten finalists in the Student Paper Contest of the 2015 International Geoscience and Remote Sensing Symposium (IGARSS), the 2016 NASA Science Team Award in Precipitation Measurement Mission (PMM) for working with GPM XCal calibration, and the 2019 ESSIC Service Award. He chairs the ESSIC Seminar Series with academic lectures delivered by distinguished scientists. He has served as an Associate Editor for IEEE ACCESS.

Hu Yang (Member, IEEE) received the Ph.D. degree from the Institute of Remote Sensing Application, Chinese Academy of Sciences, Beijing, China, in 2003.

From 2003 to 2011, he was a Senior Research Scientist with the National Satellite Meteorological Center, China Meteorological Administration, Beijing, leading the microwave instrument calibration and satellite ground application system development as the Instrument Scientist and the Program Scientist. In 2012, he joined the Earth System Science Interdisciplinary Center, University of Maryland, College Park, MD, USA, focusing on NPP/JPSS ATMS calibration/validation as a Project PI. He has authored over 40 peer-reviewed journals. His research interests include passive microwave radiometer calibration/validation, satellite geolocation, and satellite observation simulation.